Metal Dependence of Ligand Binding and Heavy-Atom Derivatization of Evolutionarily Distinct $PreQ_1$ Riboswitches

Joseph E. Wedekind, Joseph A. Liberman, Jermaine L. Jenkins, and Mohammad Salim

Contents

J.E. Wedekind (✉) • J.L. Jenkins
Department of Biochemistry & Biophysics, University of Rochester School of Medicine and Dentistry, Rochester, NY 14642, USA

Center for RNA Biology, University of Rochester School of Medicine and Dentistry, Rochester, NY 14642, USA

Structural Biology & Biophysics Facility, University of Rochester School of Medicine and Dentistry, Rochester, NY 14642, USA
e-mail: joseph.wedekind@rochester.edu

J.A. Liberman • M. Salim
Department of Biochemistry & Biophysics, University of Rochester School of Medicine and Dentistry, Rochester, NY 14642, USA

Center for RNA Biology, University of Rochester School of Medicine and Dentistry, Rochester, NY 14642, USA

V.A. Erdmann et al. (eds.), *Chemical Biology of Nucleic Acids*, RNA Technologies,
DOI 10.1007/978-3-642-54452-1_23,

Abstract Riboswitches are functional RNA elements located most frequently within the 5′-leader sequences of bacterial mRNAs. By directly binding to small molecules via an aptamer domain, a riboswitch can adapt quickly to changes in the concentration of a specific intracellular ligand, thereby establishing a feedback loop that controls gene expression. Here we discuss methods utilized in the structure determination of evolutionarily distinct classes of $preQ_1$ riboswitches known as class I and II, respectively. These riboswitches "sense" the pyrrolopyrimidine metabolite $preQ_1$—an intermediate on the biosynthetic pathway that produces the hypermodified tRNA base queuosine, which imparts translational fidelity. Herein, we describe (1) the use of isothermal titration calorimetry (ITC) to explore metal ion requirements for ligand binding and (2) modifications to crystallization media containing SO_4^{2-} or Na^+ that were necessary for phase determination using site-bound $Os(NH_3)_5^{3+}$ or Cs^+ ions, respectively. Our experience has shown that simple manipulations to the mother liquor can lead to favorable binding of the latter ions without the need to engineer metal-binding sites, thus making our methods a first-choice approach that is broadly applicable to functional RNAs.

Keywords Riboswitch • RNA crystallography • Isothermal titration calorimetry • Cesium • Osmium • Mother liquor • Heavy atom • $PreQ_1$

1 Introduction

RNA is central to life and has proven to be an exceptionally diverse molecule in terms of its functional repertoire (Serganov and Patel 2007; Clancy 2008). One activity of recent note is that certain structural elements, called riboswitches, can regulate gene expression by controlling mRNA transcription and translation (Winkler and Breaker 2003; Bastet et al. 2011) and less frequently by influencing intron excision (Kubodera et al. 2003; Lee et al. 2010; Chen et al. 2011), and mRNA stability via backbone self scission (Winkler et al. 2004); see Serganov and Nudler (2013) for a review. In the most common scenario, a riboswitch detects a small molecule that binds to its 'aptamer domain.' Such binding causes the riboswitch to undergo a conformational change that sequesters or unfurls mRNA sequences in a downstream expression platform, leading to gene "on" or "off" states (Mironov et al. 2002; Winkler et al. 2002; Nahvi et al. 2002; Sudarsan et al. 2003).

In this chapter, we review techniques used to characterize two phylogenetically unrelated riboswitches that bind the same secondary metabolite, $preQ_1$—an intermediate in the queuosine (Q) biosynthetic pathway (Fig. 1a). These riboswitches are designated class 1 ($preQ_1$-I) and class 2 ($preQ_1$-II) and were identified in the genomes of numerous bacteria within the Firmicutes phylum. $PreQ_1$-I riboswitches,

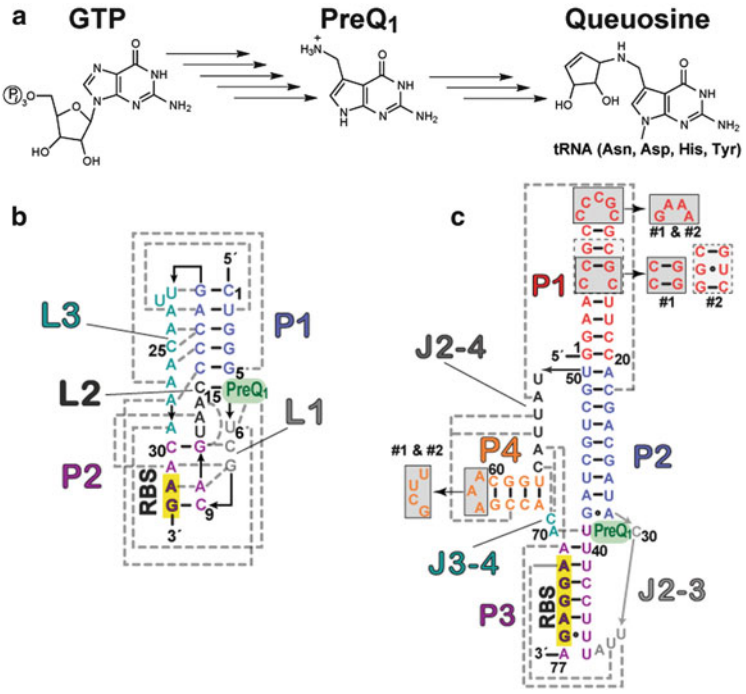

Fig. 1 Queuosine biosynthesis in bacteria and schematic structure of $preQ_1$-I and $preQ_1$-II riboswitches reviewed herein. (**a**) The bacterial biosynthetic pathway from GTP to queuosine (Q) involves several enzymes (*arrows*) that lead to the soluble intermediate $preQ_1$, which is incorporated into tRNA at that wobble position to ultimately give Q as a means to confer translational fidelity (reviewed in McCarty and Bandarian 2012). (**b**) Representative class 1 $preQ_1$ riboswitch from *Thermoanaerobacter tengcongensis* (Tte) depicting the H-type pseudoknot with tertiary hydrogen-bond interactions (*gray*) from crystal structures (Jenkins et al. 2011; Spitale et al. 2009). Watson–Crick pairs are depicted as short, *solid lines*; *arrows* indicate connectivity. The ribosome-binding site (RBS) is highlighted in *yellow*. (**c**) Representative class 2 $preQ_1$ riboswitch from *Lactobacillus rhamnosus* (Lra) depicting the HL_{out} pseudoknot. Interactions and sequence features are as described in (**b**) based on the structure (Liberman et al. 2013). Boxed regions (*gray*) show wild-type sequences that were modified to produce constructs #1 and #2, respectively

such as that from *B. subtilis*, reside in the 5′-leader sequence of the *queC* gene located in the *queCDEF* operon, which encodes enzymes essential for synthesis of $preQ_1$. $PreQ_1$-I functions as a "switch" because high cellular levels of $preQ_1$ favor metabolite binding to its aptamer domain, thus promoting formation of a rho-independent transcription terminator within its downstream expression platform. When $preQ_1$ levels are low, the expression platform forms an anti-terminator stemloop that favors gene transcription (Roth et al. 2007). Other $preQ_1$-I riboswitches appear to regulate translation, such as that from *T. tengcongensis* (Tte) (Fig. 1b). The Tte $preQ_1$-I riboswitch is located within the 5′-leader sequence of COG4708 (DUF988) mRNAs that encode a putative $preQ_1$ transporter. In the

preQ$_1$-bound state, the aptamer adopts a conformation that buries the first two bases of the ribosome-binding site (RBS), thus blocking ribosome access to the expression platform leading to attenuated gene expression. When preQ$_1$ levels are low, the block is relieved and translation ensues (Roth et al. 2007; Spitale et al. 2009; Jenkins et al. 2011). Similar feedback regulation has been ascribed to preQ$_1$-II riboswitches, such as that from *L. rhamnosus* (Fig. 1c). Such riboswitches also govern COG4708 genes (Weinberg et al. 2007) although they bury the entire RBS when preQ$_1$ binds to the aptamer (Liberman et al. 2013; Meyer et al. 2008). Because preQ$_1$ is unique to the bacterial metabolome (McCarty and Bandarian 2012), and class 1 and 2 preQ$_1$ riboswitches are present in a variety of pathogenic bacteria (Meyer et al. 2008; Roth et al. 2007; Weinberg et al. 2007), these riboswitches are of interest as antibacterial targets.

1.1 Learning Objectives of This Chapter

Here we describe approaches used to define the metal dependence of small-molecule binding to preQ$_1$ riboswitches by isothermal titration calorimetry (ITC), as well as methods employed to introduce osmium(III) pentaammine and cesium (I) heavy-atom derivatives into the class 1 and 2 preQ$_1$ riboswitches for multi-wavelength anomalous diffraction (MAD) or single-wavelength anomalous diffraction (SAD) phasing, respectively (Spitale et al. 2009; Jenkins et al. 2011; Liberman et al. 2013). The methods are written for graduate students or post-doctoral trainees with preliminary to intermediate knowledge of these topics; the information is meant as a practical guide rather than a pedagogical one. A key aspect of our methods is that they are broadly applicable to other functional RNAs and should stimulate the development of derivative approaches in the reader's laboratory.

2 Isothermal Titration Calorimetry Methods for Riboswitches

2.1 Quantitative Procedures to Test Metal Ion Requirements for Ligand Binding

Ions play a significant role in RNA folding and function. In this section, we describe methods to probe riboswitch ion requirements by measuring ligand affinity in the absence or presence of various ions. K^+ and Mg^{2+} are likely to be of greatest interest since they are prominent in the bacterial cell. K^+ concentrations range from 0.1 to 0.6 M (McLaggan et al. 1994), whereas free Mg^{2+} is present at 1–2 mM (Alatossava et al. 1985). Mg^{2+} promotes RNA folding and tertiary interactions (Pyle 2002; Draper et al. 2005; Woodson 2005) but can also impart function by participating in

the chemical reactions of ribozymes (Nakano et al. 2001; Chen et al. 2010; Toor et al. 2009; Marcia and Pyle 2012; Stahley and Strobel 2006). In the case of riboswitches, Mg^{2+} shifts the folding equilibrium of most aptamer domains into a "binding-competent" conformation that interacts with ligand (Montange and Batey 2008). Some riboswitches recognize their ligand in the absence of Mg^{2+}, such as the guanine (xptG) riboswitch (Serganov et al. 2004), the SAH riboswitch (Edwards et al. 2010), as well as the $preQ_1$-I and $preQ_1$-II translational riboswitches (Sect. 2.5 and Liberman et al. 2013); however, Mg^{2+} still drives these RNAs into a binding-competent state. In addition to imparting structural stability, some riboswitches bind synergistically to Mg^{2+} and ligands, such as the glmS, TPP, FMN, and glycine riboswitches (Klein and Ferre-D'Amare 2006; Serganov et al. 2006, 2009; Lipfert et al. 2010); see Ferre-D'Amare and Winkler (2011) for a review. Such synergy has been noted for the FMN riboswitch interaction with K^+ (Serganov et al. 2009). In addition to binding Mg^{2+}, the *Oceanobacillus iheyensis* group IIc intron selectively binds K^+ based on size, which forms part of its catalytic metal cluster (Marcia and Pyle 2012). Collectively these observations illustrate that complete characterization of a functional RNA requires analysis of the metal dependence of its activity, which should be the preface to any structural investigation.

2.2 Checking the Feasibility of Isothermal Titration Calorimetry Measurements

ITC is a quantitative method to characterize the binding thermodynamics for any two interacting molecules. This label-free approach offers a full characterization of the enthalpy (ΔH°), entropy (ΔS°), and free-energy (ΔG°) changes, as well as the equilibrium association constant, K_a; note K_a equals $1/K_d$ (the equilibrium dissociation constant). Although the approach can require large amounts of material, it is operative over a wide range of affinities between 1 mM and 1 nM. This range, however, is dictated by the respective ligand and receptor solubilities (i.e. low-affinity interactions), or what is detectable in terms of the measured heats of injection (i.e. very high-affinity interactions). Several key experimental design aspects should be considered as a preface to conducting ITC. The most important of these is the shape of the binding isotherm, which is determined by the unitless parameter c, where $c = (([M] \times n) \div K_d)$. The c value is determined by K_d, the concentration of the molecule $[M]$ in the sample cell, and the stoichiometry (n) of binding. In practice, one should strive for $20 < c < 100$ (Myszka et al. 2003) to generate measurements at the bottom, middle (inflection), and top of the titration curve; the overall shape for single-site binding should be sigmoidal. Populating the curve with data points is especially important near the inflection region since these observations are needed to accurately fit the K_a. Because we typically have an estimate of the K_d for the interaction in question, we employ the equation: $[M] = (c \times K_d) \div n$, which allows determination of the necessary molecular

concentration in the sample cell. A good starting point for the titrant concentration in the syringe is 7–10 times the value of [*M*]. Upon collecting preliminary data, this relationship should be adjusted to reach saturation. Achieving a regular baseline after each injection is important. The heat of ligand dilution following saturation may be accounted for by subtracting the average of the last three points of the saturated thermogram from the total heat of each prior injection. This will provide greater accuracy in the integrated heats that are used in nonlinear least squares curve fitting to obtain the values of ΔH°, n and K_a. Accurate knowledge of the concentrations of the molecules under investigation is imperative.

2.3 General Notes About ITC Instrument Settings

The following settings apply to a MicroCal VP-ITC system (GE Healthcare). If it has not been filled recently, or if prior experiments were run at elevated temperatures, the reference cell should be emptied and refilled with degassed, distilled H_2O. We begin investigating most binding interactions at a cell temperature of 30 °C; the temperature can be adjusted on a case-by-case basis to alter ΔH (and raw heats) to optimize the binding isotherm. A typical experiment begins with ~30 injections from a 250 µl syringe with an initial injection of 3 µL (discarded during fitting). The remaining injections are 10 µL with 20 s duration per injection. The reference power is 15 µcal s^{-1}, stirring speed 307 rpm, and the feedback mode/gain is 'high'. These settings are suitable to interrogate most macromolecular interactions (Suddala et al. 2013; Liberman et al. 2013; Salter et al. 2012). The time between injections should be sufficient for the interaction heat to return to baseline before the next injection begins; 240 s is a reasonable starting point but can be adjusted as needed. One should also strive for an average integrated heat of 3–5 µcal evolved (or absorbed) per injection for the first two-thirds of the injections. The sensitivity of the VP-ITC is about 0.1 µcal.

2.4 Preparation of Samples for ITC

The Tte $preQ_1$-I riboswitch 33-mer (Fig. 1b) was produced by chemical synthesis and HPLC purified by C18 reverse-phase separation (Wedekind and McKay 2000; Spitale et al. 2009; Spitale and Wedekind 2009). The Lra $preQ_1$-II riboswitch 77-mer (Fig. 1c) was generated by in vitro transcription and purified by denaturing PAGE (Lippa et al. 2012; Liberman et al. 2013). The $preQ_1$ ligand used for ITC analysis was prepared by chemical synthesis (LeadGen Labs, LLC). Lyophilized RNA samples were stored at −20 °C until needed. Samples were dissolved in 0.050 M Na-HEPES pH 7.0 containing 0.10 M NaCl. For $MgCl_2$-free conditions 0.5 mM EDTA at pH 7.0 was included in lieu of multivalent ions. The RNA solution was heated to 65 °C for 5 min, then $MgCl_2$ was added slowly to 6.0 mM

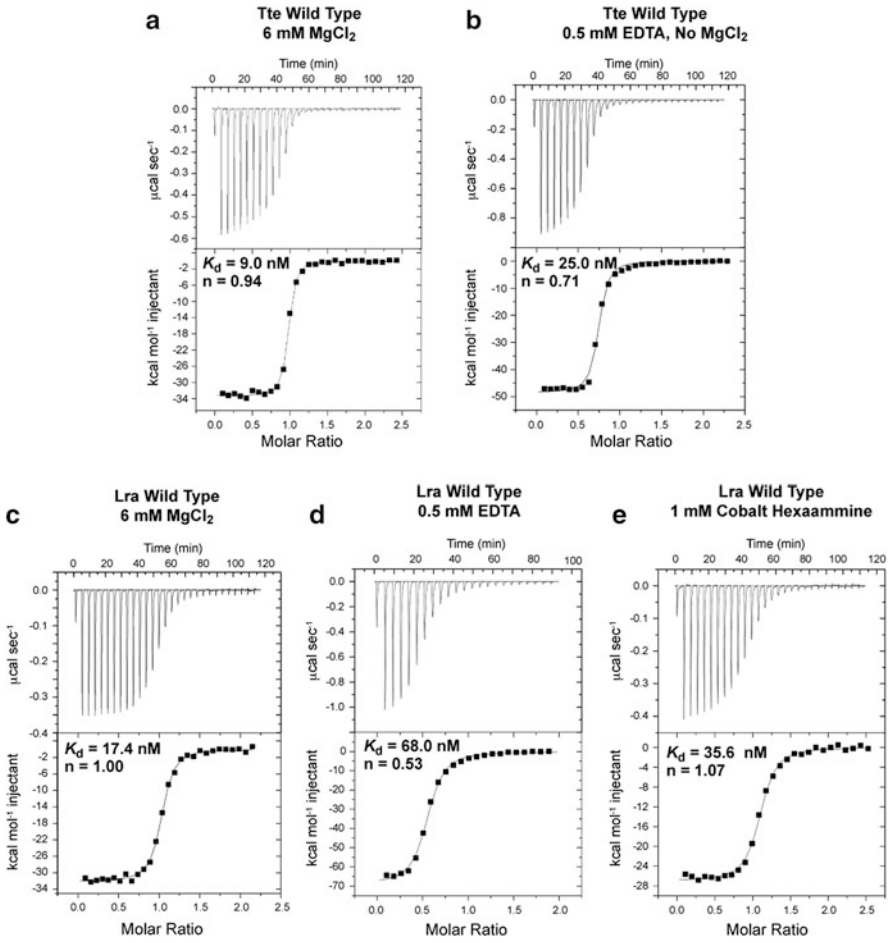

Fig. 2 Representative ITC titrations and curve fits for ligand binding to $preQ_1$-I and $preQ_1$-II riboswitches in the presence of EDTA or various Mg^{2+} or $Co(NH_3)_6^{3+}$ levels. (**a**) $PreQ_1$ interaction with the Tte 33-mer (class 1) wild-type sequence in 0.10 M NaCl, 0.006 M $MgCl_2$, and 0.050 M HEPES pH 7.0 at 25 °C; the *c* value was 522. (**b**) $PreQ_1$ binding to the Tte 33-mer under conditions in (**a**) except that $MgCl_2$ was replaced with 0.5 mM EDTA; the *c* value was 228. (**c**) $PreQ_1$ binding to the wild-type Lra 77-mer under conditions in (**a**); the *c* value was 184. (**d**) $PreQ_1$ interaction with the wild-type Lra 77-mer under conditions described in (**b**); the *c* value was 63. (**e**) $PreQ_1$ binding to the wild-type Lra riboswitch under conditions in (**a**) except that $MgCl_2$ was replaced with 0.001 M $Co(NH_3)_6Cl_3$; the *c* value was 101. In cases where $c > 100$, such values are a compromise because reduced RNA concentrations gave low heats of injection. The resulting K_d values should be treated circumspectly. The average values for two or more measurements are reported in the main text

or $Co(NH_3)_6Cl_3$ was added to 1.0 mM, followed by slow cooling to 24 °C. $MgCl_2$, and $Co(NH_3)_6Cl_3$ were omitted completely for folding conditions containing EDTA. Each riboswitch sample was dialyzed overnight at 4 °C against 4 L of

0.10 M NaCl with 6.0 mM $MgCl_2$, 1 mM $Co(NH_3)_6Cl_3$, or 0.5 mM EDTA, buffered at pH 7.0 by 0.050 M Na-HEPES. Following dialysis, samples were diluted with dialysis buffer to: 4.7 μM for the $preQ_1$-I and 3.3 μM for $preQ_1$-II wild-type riboswitches; 5.7 μM for the $preQ_1$-I and 1.5–5.7 μM for wild-type sequences folded in 0.5 mM EDTA; and 3.6 μM for wild-type $preQ_1$-II with $Co(NH_3)_6Cl_3$. $PreQ_1$ was dissolved in dialysis buffer to a concentration tenfold higher than the RNA.

ITC measurements were conducted by syringe injection of $preQ_1$ into a sample cell containing the riboswitch (cell volume ~1.7 mL) using 28 or 29 injections of 10 μL each—except for the first 3 μL injection. An interval of 120 or 260 s was used between injections. Thermograms were analyzed with Origin 7.0 (MicroCal) using a 1:1 binding model. Experiments for publication should be performed at least twice. Representative titrations and curve fits are in Fig. 2.

2.5 *Outcomes for Metal Dependence of Ligand Binding Based on ITC*

Previously we demonstrated that the wild-type Tte $preQ_1$-I riboswitch binds $preQ_1$ with an affinity of 2.1 ± 0.3 nM using surface plasmon resonance (SPR). This method required 5′-biotinylation of the RNA aptamer for immobilization to an SPR chip (Jenkins et al. 2011). SPR was conducted in 0.010 M Na-cacodylate pH 7.0 containing 3 mM $MgCl_2$ at 25 °C. A comparable K_d of 7.4 ± 2.3 nM was measured at pH 7.0 in 6 mM $MgCl_2$ with an average n value of 0.98 ± 0.07 (Fig. 2a and Suddala et al. 2013). To test the metal-ion dependence of ligand binding, the Tte RNA was folded in 0.5 mM EDTA in place of metals. The resulting K_d of 25.0 nM (Fig. 2b) suggested that $MgCl_2$ was not required for ligand binding but the relatively low n value of 0.7 suggested that a significant portion of the riboswitch does not adopt a binding-competent conformation. A similar trend was observed for the Lra $preQ_1$-II riboswitch in which average K_d values for $preQ_1$ binding were 17.9 ± 0.6 nM and 72.5 ± 6.3 nM in the presence and absence of Mg^{2+}, respectively (Fig. 2c, d and Liberman et al. 2013). Despite a modest factor-of-four decrease in affinity, the average n value in the presence of EDTA was 0.57 ± 0.05, suggesting that slightly more than half of the riboswitch adopts a $preQ_1$ binding-competent state. In this manner, the ion dependence of ligand binding can be explored, as well as the need for inner-sphere or outer-sphere interactions (reviewed in Wedekind 2011). For example, the crystal structure showed Mg^{2+} binding by the $preQ_1$-II riboswitch via inner- and outer-sphere contacts (Liberman et al. 2013). However, ITC measurements indicated $Co(NH_3)_6^{3+}$ can substitute for Mg^{2+} in ligand binding (Fig. 2e), based on a minimal increase in K_d. This result suggests inner-sphere ion coordination is not a strict requirement for $preQ_1$ binding (Liberman et al. 2013).

3 General Approaches to Introduce Heavy Atoms into Riboswitches

3.1 Mother Liquor Manipulations to Promote Heavy Atom Binding

For novel RNA folds, it is often necessary to determine phases for the measured structure factor amplitudes (F_{obs}) by use of experimental approaches. This requires an empirical search for conditions that lead to the identification of one or more "heavy atom" binding sites that can be used to establish phases for the non-hydrogen RNA atoms (Wedekind and McKay 2000). For the $preQ_1$-I and $preQ_1$-II riboswitches, determination of the respective phases presented unique challenges that required manipulation of the mother liquor to promote heavy atom binding (Spitale and Wedekind 2009; Liberman et al. 2013). $PreQ_1$-I riboswitch crystals grew from high-salt mother liquors containing the negatively charged SO_4^{2-} ion, which competes with the RNA for binding $Os(NH_3)_5^{3+}$ and variants thereof, thus requiring sulfate removal from crystals. By contrast, the poor reproducibility of $preQ_1$-II crystals—approximately one useful crystal for every seven screened for X-ray diffraction—required co-crystallization of Cs^+ with the riboswitch in order to determine the structure by use of single-crystal approaches. Here we review techniques that assisted heavy-atom binding and ultimately led to high-resolution structure determinations of these, heretofore unknown, RNA folds.

3.2 Eliminating SO_4^{2-} to Promote $Os(NH_3)_5^{3+}$ Binding

High-salt mother liquors are useful to grow RNA crystals but can predispose subsequent heavy atom-derivative searches to grave failure. Although strategic placement of halogenated pyrimidines can assist with heavy-atom phasing (Golden 2000; Pley et al. 1994; Correll et al. 1997b), there are examples in which high-salt mother liquors have been supplanted by low ionic strength conditions that favor site-specific ion binding due to reduced electrostatic shielding. Such changes can be made at the level of RNA crystal growth or by in situ methods that entail slow replacement of salt within the crystal. In the case of the minimal hairpin ribozyme, crystals could be grown from solutions of 1.8 M $(NH_4)_2SO_4$ as well as lower ionic strength 0.25 M Li_2SO_4 supplemented with 22–24 % (w/v) poly(ethylene) glycol 2000 monomethyl ether (Alam et al. 2005).

By contrast, useful $preQ_1$-I riboswitch crystals grew only from solutions of 1.8 M Li_2SO_4 (Spitale et al. 2009). Although a well diffracting, low-ionic-strength crystal form grew from 2-methyl-2,4-pentanediol (Lippa et al. 2012), merohedral twinning thwarted phasing attempts (Torelli 2008). Efforts to prepare heavy-atom

derivatives of the Li_2SO_4 crystal form using halogenated pyrimidines and heavy-atom soaks proved unsuccessful. To overcome the limited solubility and poor reactivity of heavy-atom compounds in the high-salt mother liquor, crystals were first placed into a "stabilization" solution comprising 2.0 M Li_2SO_4, 0.10 M Na-cacodylate pH 6.0, 0.02 M $MgSO_4$, 5 % (v/v) 1,3-propanediol, 2 mM spermine, and saturating amounts of ligand. Crystals were then serially transferred into a "derivative" solution of 4.0 M LiOAc, 0.02 M $Mg(OAc)_2$, 0.10 M Na-cacodylate pH 6.5, 5 % (v/v) 1,3-propanediol, 2 mM spermine, saturating ligand, and 0.10 M pentaammine-(trifluoro-methane-sulfonato) Os(III) triflate (Sigma-Aldrich). Our rationale was that we previously grew hammerhead ribozyme crystals from 1.9 to 2.2 M NH_4SO_4 as well as 3.2 M KOAc (Wedekind and McKay 2000), suggesting that both anions were compatible with crystals. Additionally, sulfate adopts multiple modes of metal coordination via uni- or bidentate interactions (Cotton and Wilkinson 1988) and is known to produce insoluble group II and transition-metal complexes. By contrast, acetate coordinates unidentately making it a relatively weak metal binder.

During the exchange of SO_4^{2-} with OAc^-, we maintained constant ionic strength by assuming 4.0 M LiOAc was equivalent to 2.0 M $Li_2(SO_4)$. The exchange solutions were mixed in the following derivative-to-stabilizing solution ratios: 1:3, 1:1, and 3:1; each transfer lasted 15 min and crystals showed no signs of osmotic shock. After the final crystal transfer into the derivative solution, crystals were incubated for 3 h. High acetate concentrations also serve as a cryoprotectant (Wedekind and McKay 2000), which allowed samples to be flash frozen directly by plunging into $N_2(l)$. MAD phasing of $preQ_1$-I crystals has been described elsewhere (Spitale et al. 2009).

3.3 *The Mode of $Os(NH_3)_5^{3+}$ Binding to the $PreQ_1$-I Riboswitch*

Inspection of the $preQ_1$-I riboswitch structure revealed the mode of $Os(NH_3)_5^{3+}$ binding to RNA (Spitale et al. 2009). Anomalous difference Fourier maps revealed two binding sites: a minor site at the sugar edge of Uri21 and a major site on the twofold axis between $preQ_1$-I riboswitch molecules (Fig. 3). The latter doubly weighted peak had a 30 σ height and the ion received coordination from six oxygens. Due to the isotropy of pentaammine binding, it was not possible to discern the identity of the sixth, inner-sphere ligand in the osmium coordination sphere; such spatial averaging is not always the case (Cate and Doudna 1996). Notably, our observations differ from osmium(III) hexammine binding to the P4–P6 domain of the group I intron, which involved binding at tandem G•U wobble base pairs (Cate and Doudna 1996). Similar G•U binding modes were reported for $Ir(NH_3)_6^{3+}$ in a comprehensive analysis of major-groove ion binding motifs (Keel et al. 2007); at present, it is unclear whether $Os(NH_3)_5^{3+}$ can bind G•U pairs in the manner

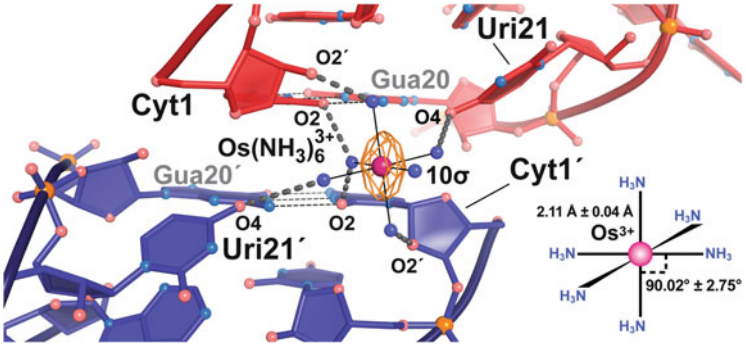

Fig. 3 Site-bound Os(III) at the dyad interface of the Tte preQ$_1$-I riboswitch. The outer-sphere Os$(NH_3)_5^{3+}$ amines bind to the riboswitch via interactions with the O2-keto and O2′ sugar of Cyt1, as well as O4 keto contacts from Uri21 (*red model*). Because the Os$(NH_3)_5^{3+}$ resides on a proper twofold axis, these interaction are duplicated by a symmetry-related molecule (*blue model*) denoted by a prime (′). The anomalous difference electron density map (*orange mesh*) is contoured at 10σ. (*Inset*) The average octahedral geometry for Os$(NH_3)_6^{3+}$ (reviewed in Wedekind 2011)

documented for hexammine ions. Nonetheless, we favor pentaammine-(trifluoromethane-sulfonato) Os(III) triflate as a first choice RNA derivative because it is site selective, commercially available, does not require G•U pairs in the sequence, and circumvents the need for in-house synthesis of Os$(NH_3)_6^{3+}$ or Ir$(NH_3)_6^{3+}$ (reviewed in Wedekind 2011).

3.4 *Co-crystallization with Cs^+ for Single-Wavelength Anomalous Diffraction Phasing*

To identify crystals of the preQ$_1$-II riboswitch, we screened sequences from several species including: *Streptococcus gordonii*, *S. pneumoniae*, *Lactobacillus casei*, and *L. rhamnosus*. The best X-ray-diffraction-quality crystals grew from a modified variant of the *L. rhamnosus* sequence (Lippa et al. 2012; Liberman et al. 2013) in which nonconserved stem loops in P1 and P4 were replaced with stable GNRA and UNCG tetraloops, respectively (Fig. 1c, construct #1) (Liberman et al. 2013). In another variation, P1 was modified to include a G•U wobble (Fig. 1c, construct #2) that was shown to function as a phasing module due to its avidity for Os$(NH_3)_6^{3+}$, Ir$(NH_3)_6^{3+}$ or Cs^+ (Keel et al. 2007). Constructs #1 and #2 yielded crystals by the vapor-diffusion method from solutions of: 14.4–14.8 % (*w*/*v*) poly(ethylene) glycol 6000 (PEG6K), 0.14–0.16 M $MgOAc_2$, 0.05 M Na-cacodylate pH 6.0, 1–2 mM spermine, and 0.20 M NaCl. Crystals appeared at 20 °C and grew as rectangular plates to 0.20 mm × 0.05 mm × 0.02 mm within 2–3 weeks. Cryo-protection was achieved by a 30 s transfer into synthetic mother liquor comprising: 17.2–17.8 % (*w*/*v*) PEG6K, 168-192 mM $MgOAc_2$, 0.24 M NaCl, 0.06 M Na-cacodylate pH 6.0,

and 1.2 mM spermine supplemented with 20 % (*v*/*v*) 2-methyl-2,4-pentanediol and 20 % (*v*/*v*) ethanol. The best crystals diffracted in house to 2.8 Å resolution and were stored in $N_2(l)$ dewars prior to X-ray diffraction data collection. Diffraction analysis revealed that construct #1 belonged to space group $C222_1$ with one molecule per asymmetric unit ($a = 58.0$ Å, $b = 86.0$ Å, $c = 98.1$ Å and $\alpha = \beta = \gamma = 90°$) (Liberman et al. 2013). Construct #2 crystallized in space group $P2_1$ with four molecules per asymmetric unit ($a = 83.6$ Å, $b = 60.7$ Å, $c = 101.5$ Å and $\alpha = \gamma = 90°$ with $\beta = 106.8°$) (Liberman, Salim and Wedekind, unpublished).

Although substantial effort was expended to prepare heavy-atom derivatives, both crystal forms were recalcitrant to derivatization. One obstacle was that only one in seven crystals from the same drop exhibited useful X-ray diffraction, which hindered efforts to generate a starting supply of crystals that could be subjected to heavy-atom screening. Another shortcoming was a paucity of $Ir(NH_3)_6^{3+}$ binding based on the absence of a measurable anomalous signal. The latter phenomenon was most likely the result of elevated Mg^{2+} concentrations in mother liquors that were necessary to obtain high-quality X-ray diffraction. Even though construct #2 possessed a G•U wobble, it had no appreciable $Ir(NH_3)_6^{3+}$ binding.

To surmount difficulties, we undertook co-crystallization in the presence of CsCl in lieu of NaCl. Substitution of Na^+ with Cs^+ caused no apparent changes in space group despite notable differences between these ions. Cs^+ is electron rich (54 e^-) relative to Na^+ (10 e^-) and forms as many as 11 inner-sphere contacts. A search of the Cambridge Structural Database (Allen 2002) version 5.34 using ConQuest v1.15 (Bruno et al. 2002) revealed an average Cs^+ to O–C distance of 3.23 ± 0.16 Å, an average Cs^+ to N–C distance of 3.31 ± 0.15 Å, (where the O–C and N–C bond was of any type), and an average Cs^+ to water distance of 3.27 ± 0.16 Å. Such distances are significantly longer than those for Na^+ to O–C, as well as K^+ to O–C, which exhibited values of 2.53 ± 0.17 and 2.83 ± 0.08 Å, respectively.

The presence of Cs^+ improved the resolution of X-ray diffraction for $preQ_1$-II crystals, as well as the reproducibility of well-diffracting crystals. Of particular significance is the fact that Cs^+ exhibits a +9 electron anomalous-diffraction signal (f'') at 1.70 Å resolution, which enabled use of the site-bound Cs^+ ions of construct #1 as a means to generate high-quality SAD phases for a complete structure determination (Liberman et al. 2013). By comparison, the low-symmetry space group of construct #2 crystals hampered collection of the anomalous signal, preventing an independent structure determination. Nonetheless, the latter structure was solved by molecular replacement, which yielded the locations of a number of Cs^+ ions whose identities were corroborated by anomalous difference Fourier maps (Liberman, Salim and Wedekind, unpublished). We also conducted co-crystallization of the Lra $preQ_1$-II riboswitch from Br^- and I^- salts in lieu of Cl^-. The latter ions produced well diffracting crystals using Na^+ as a counter ion, but no significant anomalous diffraction signal was detected. Our results suggest that halide salts are not useful for RNA phasing, in contrast to proteins (Dauter and Dauter 2001).

3.5 *The Binding Mode of Cs^+ to a G•U Wobble Pair and Other Sites*

We included a single-site G•U wobble pair in stem P1 of the $preQ_1$-II riboswitch with the goal of using it as a phasing module (Fig. 1c, construct #2). This approach was described in a thorough analysis on the propensity of single and tandem G•U wobble sites to bind $Os(NH_3)_6^{3+}$ or $Ir(NH_3)_6^{3+}$ for heavy-atom phasing (Keel et al. 2007). We chose the sequence 5′-GGC-3′/3′-CUG-5′, which features a single-wobble pair, dubbed phasing module 14 (PM14) (Keel et al. 2007). PM14 was stated to have advantages over other G•U motifs including (1) metal binding with one of the highest anomalous signals and lowest B-factors relative to a reference hexammine site and (2) inclusion of a single wobble requires only three nucleotides to be altered in the target RNA sequence rather than four (Keel et al. 2007). It was also noted that the G•U wobble of PM14 binds Cs^+, which proved useful in phasing the SAM-II riboswitch wherein NH_4^+ in the mother liquor was replaced with Cs^+, introduced by crystal soaking (Keel et al. 2007; Gilbert et al. 2008). As noted above, the $preQ_1$-II riboswitch was co-crystallized with 0.15 M Cs^+ yielding 15 site-bound Cs^+ ions in construct #1 (one molecule per asymmetric unit) (Liberman et al. 2013) and 35 Cs^+ ions in construct #2 (four molecules per asymmetric unit) (Liberman, Salim and Wedekind, unpublished).

The strongest anomalous difference Fourier signal in electron density maps was observed for Cs^+ bound at the G•U wobble of construct #2; the average peak height was 21 ± 2 σ δ for all four riboswitch copies in the asymmetric unit. Because construct #1 did not possess such a phasing module (Fig. 1c), Cs^+ was not detected at a spatially equivalent location. Cs^+ coordination at the G•U wobble site of construct #2 entailed contacts in the P1 major groove (Fig. 4a), which concur with the mode of Cs^+ coordination at PM14 in the SAM-II riboswitch (Gilbert et al. 2008). A variety of other single G•U wobble pairs have been reported to bind Cs^+ including: 5′-GGA-3′/3′-CUG-5′ in the lysine riboswitch (Serganov et al. 2008); 5′-GGA-3′/3′-CUU-5′ in the FMN riboswitch (Serganov et al. 2009); as well as 5′-GGU-3′/3′-CUA-5′ and 5′-CGU-3′/3′-GUA-5′ from the *O. iheyensis* group IIc intron (Marcia and Pyle 2012). Each of the latter, site-bound ions was introduced by soaking crystals in solutions of Cs^+. (Wobble sites engaged in tertiary or crystal contacts were not considered in the sequences above).

The low-symmetry $P2_1$ space group of our $preQ_1$-II riboswitch (construct #2) contains four molecules per asymmetric unit, which impeded high-resolution SAD phasing. As such, we focused on the higher symmetry $C222_1$ space group of construct #1, which proved successful despite the absence of a G•U pair for ion binding. Serendipitous Cs^+ binding prompted us to ask (1) *what sequences common to both preQ$_1$-II constructs exhibited appreciable levels of Cs^+ binding based on the measurable anomalous signal?* and (2) *which of the latter Cs^+ sites are present in secondary structure that does not strictly depend upon tertiary or crystal contacts for ion binding?* Of the 15 Cs^+ sites identified and modeled in the structure of construct #1, the average anomalous peak height was 8.9 σ and the average

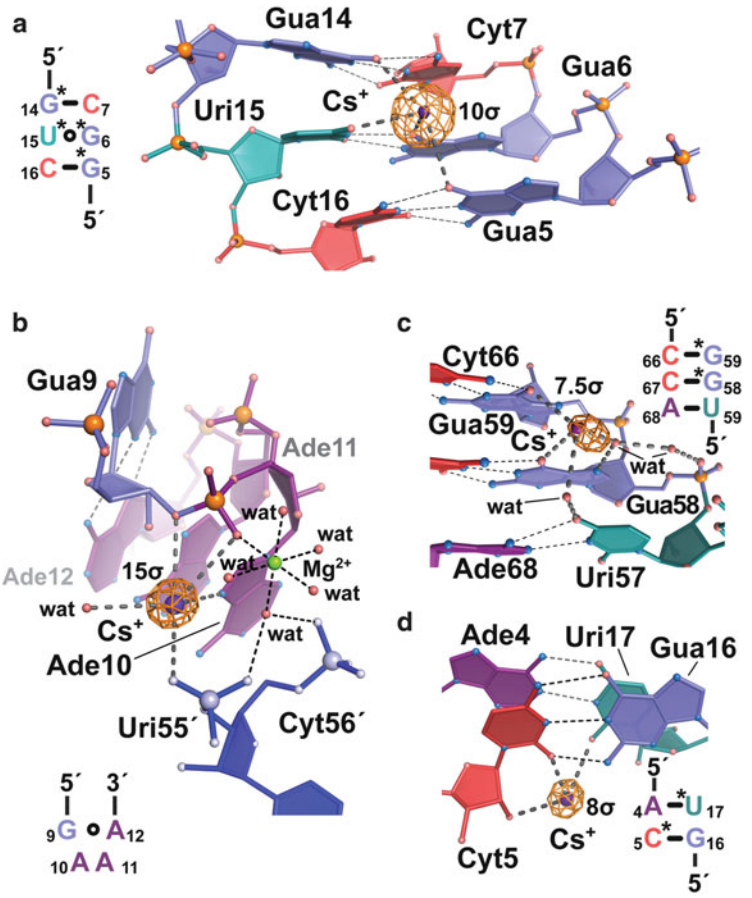

Fig. 4 Representative site-bound Cs^+ ions in the Lra preQ$_1$-II riboswitch G•U wobble, GNRA tetraloop and secondary structures with accompanying anomalous difference Fourier maps. (**a**) The mode of G•U wobble coordination to Cs^+ in construct #2 entails inner-sphere contacts with the keto oxygens of Gua5, 6 and 14, and Uri15 in the P1 major groove. Here and elsewhere the secondary structure is shown; *asterisks* (*) indicate base keto-oxygen coordination to Cs^+. (**b**) GNRA tetraloop coordination to Cs^+ utilizes N7 of Ade10, O3′ of Gua9, and nonbridging phosphate oxygens from Ade10 and Uri55′; the latter interaction arises from a crystal contact (blue ball-and-stick-model). A nearby Mg^{2+} shows inner-sphere coordination to the nonbridging phosphate oxygen from Ade10. (**c**) Major groove Cs^+ binding by tandem Gua bases. The O6 groups of Gua58 and Gua59 make inner-sphere Cs^+ contacts whereas N7 of Gua58 and the O4 keto of Uri57 serve to position waters for ion coordination. (**d**) Minor groove Cs^+ binding at the sugar-edge of Cyt5. Coordination entails the O2 keto and 2′-O groups of Cyt5 and the cross-strand O2 keto group of Uri17

refined *B*-factor was 43 Å^2. Our results revealed the highest occupancy and largest anomalous signal for Cs^+ at Ade10, which resides in apposition to the phosphodiester bond between Gua9 and Ade10 within the GNRA tetraloop that caps P1 (Fig. 4b). This site has an average peak height of 17.4 ± 3.5 σ based on all

five molecules of constructs #1 and #2. The strong occupancy is likely derived from four inner-sphere contacts originating from three GNRA ligands, as well as a nonbridging phosphate oxygen donated by a crystal contact (Fig. 4b). A nearby Mg^{2+} coordinates to the backbone of Ade10, which simultaneously makes an inner-sphere contact to the GNRA-bound Cs^+. Mg^{2+} aside, a similar constellation of Cs^+ ligands was observed in the GNRA tetraloop of the *O. iheyensis* group IIc intron, including N7 of base Ade33 in the "N" position of the tetraloop (Marcia and Pyle 2012). Like the preQ$_1$-II riboswitch, the coordination sphere of this ion is completed by inner-sphere coordination to a crystal contact, which draws into question the generality of the GAAA motif as a "sure-fire" Cs^+-binding site.

Two other Cs^+ sites were prominent in preQ$_1$-II structures of constructs #1 and #2. Both sites are located in helical regions devoid of tertiary or crystal contacts. The first site was bound in the major groove of P4 at the sequence 5′-UGG-3′/3′-ACC-5′. The average height of the anomalous difference Fourier peak was 4.9 ± 2.8 σ. Here, tandem Gua bases appear important in Cs^+ binding (Fig. 4c). A comparable mode of coordination is observed at the base of a GNRA tetraloop in the *O. iheyensis* group IIc intron in the sequence 5′-UGG-3′/3′-ACA-5′, wherein the G•A pair corresponds to the first and last residues of a GNRA tetraloop. Specifically, Gua275 at position *i* of the tetraloop forms a sheared pair with Ade278 at position *i* + *3*. The keto oxygens of the sequence 5′-UGG-3′ each make inner-sphere contacts to Cs^+ (Marcia and Pyle 2012).

The involvement of O6 groups from tandem guanines to coordinate Cs^+ has also been observed at Gua29/30 of the *O. iheyensis* group IIc intron (Marcia and Pyle 2012). Other tandem Gua sequences are present but these make prominent use of tertiary contacts for ion binding. Tandem Gua nucleobases—specifically tandem G•U wobbles—have long been known as hotspots for hexammine binding (Cate and Doudna 1996; Keel et al. 2007). Moreover, tandem Gua bases in RNA duplexes—outside the context of wobbles—are known to be sites of $Mg(H_2O)_6^{2+}$ coordination (Correll et al. 1997a; Jovine et al. 2000; Shi and Moore 2000; Wedekind and McKay 2003). Our work and that of others suggests that such sequences bind Cs^+, although binding is not necessarily mutually exclusive with respect to $Mg(H_2O)_6^{2+}$ based on respective *O. iheyensis* group IIc intron structures soaked in Li^+/Mg^{2+} and Cs^+/Mg^{2+} (Marcia and Pyle 2012).

A second sequence-specific Cs^+ binding site was located in the minor groove of preQ$_1$-II constructs #1 and #2 (Fig. 4d). This site entailed sugar-edge binding at Cyt5 and Cyt16, respectively. In construct #1, Cs^+ bound to Cyt5 with an anomalous difference Fourier peak height of 9.9 σ. In construct #2, Cs^+ bound to Cyt16 in all four copies in the asymmetric unit with an average peak height of 4.5 ± 1.8 σ. Differences in Cs^+ localization were the result of sequence differences resulting from use of the PM14 G•U wobble (Fig. 1c). The site of Cs^+ binding in construct #1 is 5′-AC-3′/3′-UG-5′, whereas that of construct #2 is 5′-AG-3′/3′-UC-5′. At present, it is unclear what features surrounding the respective Cyt nucleobases are important for Cs^+ localization since not all accessible 5′-AC-3′ and 5′-CU-3′ sequences in

preQ$_1$-II riboswitch structures coordinate Cs^+. Higher resolution diffraction is needed to clarify this issue.

Acknowledgments We thank C. Kielkopf and J. Bogue for helpful discussions. J.A.L. was funded in part by NIH training grant T32 GM068411 and a Hooker graduate fellowship. This research was funded by NIH grants RR026501 and GM063162 to J.E.W. Portions of this research were carried out at the Stanford Synchrotron Radiation Lightsource (SSRL) and the Macromolecular Cornell High-Energy Synchrotron Source (MacCHESS). SSRL is a Directorate of SLAC National Accelerator Laboratory and an Office of Science User Facility operated for the U.S. DOE by Stanford University. The SSRL Structural Molecular Biology Program is supported by the DOE Office of Biological and Environmental Research and by NIH grants GM103393 and RR001209. MacCHESS is supported by NSF grant DMR-0936384 and NIH grant GM103485.

References

Alam S, Grum-Tokars V, Krucinska J et al (2005) Conformational heterogeneity at position U37 of an all-RNA hairpin ribozyme with implications for metal binding and the catalytic structure of the S-turn. Biochemistry 44:14396–14408

Alatossava T, Jutte H, Kuhn A et al (1985) Manipulation of intracellular magnesium content in polymyxin B nonapeptide-sensitized *Escherichia coli* by ionophore A23187. J Bacteriol 162:413–419

Allen FH (2002) The Cambridge Structural Database: a quarter of a million crystal structures and rising. Acta Crystallogr B 58:380–388

Bastet L, Dube A, Masse E et al (2011) New insights into riboswitch regulation mechanisms. Mol Microbiol 80:1148–1154

Bruno IJ, Cole JC, Edgington PR et al (2002) New software for searching the Cambridge Structural Database and visualizing crystal structures. Acta Crystallogr B 58:389–397

Cate JH, Doudna JA (1996) Metal-binding sites in the major groove of a large ribozyme domain. Structure 4:1221–1229

Chen JH, Yajima R, Chadalavada DM et al (2010) A 1.9 Å crystal structure of the HDV ribozyme precleavage suggests both Lewis acid and general acid mechanisms contribute to phosphodiester cleavage. Biochemistry 49:6508–6518

Chen AG, Sudarsan N, Breaker RR (2011) Mechanism for gene control by a natural allosteric group I ribozyme. RNA 17:1967–1972

Clancy S (2008) RNA functions. Nat Educ 1(1):102

Correll CC, Freeborn B, Moore PB et al (1997a) Metals, motifs, and recognition in the crystal structure of a 5S rRNA domain. Cell 91:705–712

Correll CC, Freeborn B, Moore PB et al (1997b) Use of chemically modified nucleotides to determine a 62-nucleotide RNA crystal structure: a survey of phosphorothioates, Br, Pt and Hg. J Biomol Struct Dyn 15:165–172

Cotton FA, Wilkinson G (1988) Advanced inorganic chemistry, 5th edn. Wiley, New York

Dauter Z, Dauter M (2001) Entering a new phase: using solvent halide ions in protein structure determination. Structure 9:R21–R26

Draper DE, Grilley D, Soto AM (2005) Ions and RNA folding. Annu Rev Biophys Biomol Struct 34:221–243

Edwards AL, Reyes FE, Heroux A et al (2010) Structural basis for recognition of S-adenosylhomocysteine by riboswitches. RNA 16:2144–2155

Ferre-D'Amare AR, Winkler WC (2011) The roles of metal ions in regulation by riboswitches. Met Ions Life Sci 9:141–173

Gilbert SD, Rambo RP, Van Tyne D et al (2008) Structure of the SAM-II riboswitch bound to S-adenosylmethionine. Nat Struct Mol Biol 15:177–182

Golden BL (2000) Heavy atom derivatives of RNA. Methods Enzymol 317:124–132

Jenkins JL, Krucinska J, McCarty RM et al (2011) Comparison of a $preQ_1$ riboswitch aptamer in metabolite-bound and free states with implications for gene regulation. J Biol Chem 286:24626–24637

Jovine L, Djordjevic S, Rhodes D (2000) The crystal structure of yeast phenylalanine tRNA at 2.0 Å resolution: cleavage by Mg^{2+} in 15-year old crystals. J Mol Biol 301:401–414

Keel AY, Rambo RP, Batey RT et al (2007) A general strategy to solve the phase problem in RNA crystallography. Structure 15:761–772

Klein DJ, Ferre-D'Amare AR (2006) Structural basis of glmS ribozyme activation by glucosamine-6-phosphate. Science 313:1752–1756

Kubodera T, Watanabe M, Yoshiuchi K et al (2003) Thiamine-regulated gene expression of Aspergillus oryzae thiA requires splicing of the intron containing a riboswitch-like domain in the 5′-UTR. FEBS Lett 555:516–520

Lee ER, Baker JL, Weinberg Z et al (2010) An allosteric self-splicing ribozyme triggered by a bacterial second messenger. Science 329:845–848

Liberman JA, Salim M, Krucinska J et al (2013) Structure of a class II $preQ_1$ riboswitch reveals ligand recognition by a new fold. Nat Chem Biol 9:353–355

Lipfert J, Sim AY, Herschlag D et al (2010) Dissecting electrostatic screening, specific ion binding, and ligand binding in an energetic model for glycine riboswitch folding. RNA 16:708–719

Lippa GM, Liberman JA, Jenkins JL et al (2012) Crystallographic analysis of small ribozymes and riboswitches. Methods Mol Biol 848:159–184

Marcia M, Pyle AM (2012) Visualizing group II intron catalysis through the stages of splicing. Cell 151:497–507

McCarty RM, Bandarian V (2012) Biosynthesis of pyrrolopyrimidines. Bioorg Chem 43:15–25

McLaggan D, Naprstek J, Buurman ET et al (1994) Interdependence of K^+ and glutamate accumulation during osmotic adaptation of *Escherichia coli*. J Biol Chem 269:1911–1917

Meyer MM, Roth A, Chervin SM et al (2008) Confirmation of a second natural $preQ_1$ aptamer class in *Streptococcaceae bacteria*. RNA 14:685–695

Mironov AS, Gusarov I, Rafikov R et al (2002) Sensing small molecules by nascent RNA: a mechanism to control transcription in bacteria. Cell 111:747–756

Montange RK, Batey RT (2008) Riboswitches: emerging themes in RNA structure and function. Annual Rev Biophysics 37:117–133

Myszka DG, Abdiche YN, Arisaka F et al (2003) The ABRF-MIRG'02 study: assembly state, thermodynamic, and kinetic analysis of an enzyme/inhibitor interaction. J Biomol Tech 4:247–269

Nahvi A, Sudarsan N, Ebert MS et al (2002) Genetic control by a metabolite binding mRNA. Chem Biol 9:1043–1049

Nakano S, Proctor DJ, Bevilacqua PC (2001) Mechanistic characterization of the HDV genomic ribozyme: assessing the catalytic and structural contributions of divalent metal ions within a multichannel reaction mechanism. Biochemistry 40:12022–12038

Pley HW, Flaherty KM, McKay DB (1994) Three-dimensional structure of a hammerhead ribozyme. Nature 372:68–74

Pyle AM (2002) Metal ions in the structure and function of RNA. J Biol Inorg Chem 7:679–690

Roth A, Winkler WC, Regulski EE et al (2007) A riboswitch selective for the queuosine precursor $preQ_1$ contains an unusually small aptamer domain. Nat Struct Mol Biol 14:308–317

Salter JD, Lippa GM, Belashov IA et al (2012) Core-binding factor beta increases the affinity between human Cullin 5 and HIV-1 Vif within an E3 ligase complex. Biochemistry 51:8702–8704

Serganov A, Nudler E (2013) A decade of riboswitches. Cell 152:17–24

Serganov A, Patel DJ (2007) Ribozymes, riboswitches and beyond: regulation of gene expression without proteins. Nat Rev Genet 8:776–790
Serganov A, Yuan YR, Pikovskaya O et al (2004) Structural basis for discriminative regulation of gene expression by adenine- and guanine-sensing mRNAs. Chem Biol 11:1729–1741
Serganov A, Polonskaia A, Phan AT et al (2006) Structural basis for gene regulation by a thiamine pyrophosphate-sensing riboswitch. Nature 441:1167–1171
Serganov A, Huang L, Patel DJ (2008) Structural insights into amino acid binding and gene control by a lysine riboswitch. Nature 455:1263–1267
Serganov A, Huang L, Patel DJ (2009) Coenzyme recognition and gene regulation by a flavin mononucleotide riboswitch. Nature 458:233–237
Shi H, Moore PB (2000) The crystal structure of yeast phenylalanine tRNA at 1.93 Å resolution: a classic structure revisited. RNA 6:1091–1105
Spitale RC, Wedekind JE (2009) Exploring ribozyme conformational changes with X-ray crystallography. Methods 49:87–100
Spitale RC, Torelli AT, Krucinska J et al (2009) The structural basis for recognition of the $PreQ_0$ metabolite by an unusually small riboswitch aptamer domain. J Biol Chem 284:11012–11016
Stahley MR, Strobel SA (2006) RNA splicing: group I intron crystal structures reveal the basis of splice site selection and metal ion catalysis. Curr Opin Struct Biol 16:319–326
Sudarsan N, Barrick JE, Breaker RR (2003) Metabolite-binding RNA domains are present in the genes of eukaryotes. RNA 9:644–647
Suddala KC, Rinaldi AJ, Feng J et al (2013) Single transcriptional and translational $preQ_1$ riboswitches adopt similar pre-folded ensembles that follow distinct folding pathways into the same ligand-bound structure. Nucleic Acid Res 41:10462–10475
Toor N, Keating KS, Pyle AM (2009) Structural insights into RNA splicing. Curr Opin Struct Biol 19:260–266
Torelli AT (2008) Structural studies of transition-state stabilization by a small catalytic RNA, metabolite-binding by a regulatory RNA sequence and the mechanism of action of activation induced deaminase. Ph.D. Dissertation, University of Rochester, School of Medicine and Dentistry, Rochester, NY
Wedekind JE (2011) Metal ion binding and function in natural and artificial small RNA enzymes from a structural perspective. Met Ions Life Sci 9:299–345
Wedekind JE, McKay DB (2000) Purification, crystallization, and X-ray diffraction analysis of small ribozymes. Methods Enzymol 317:149–168
Wedekind JE, McKay DB (2003) Crystal structure of the leadzyme at 1.8 A resolution: metal ion binding and the implications for catalytic mechanism and allo site ion regulation. Biochemistry 42:9554–9563
Weinberg Z, Barrick JE, Yao Z et al (2007) Identification of 22 candidate structured RNAs in bacteria using the CMfinder comparative genomics pipeline. Nucleic Acid Res 35:4809–4819
Winkler WC, Breaker RR (2003) Genetic control by metabolite-binding riboswitches. Chembiochem 4:1024–1032
Winkler W, Nahvi A, Breaker RR (2002) Thiamine derivatives bind messenger RNAs directly to regulate bacterial gene expression. Nature 419:952–956
Winkler WC, Nahvi A, Roth A et al (2004) Control of gene expression by a natural metabolite-responsive ribozyme. Nature 428:281–286
Woodson SA (2005) Metal ions and RNA folding: a highly charged topic with a dynamic future. Curr Opin Chem Biol 9:104–109